PHYSICAL REVIEW B **106**, 165416 (2022)

Switchable single-molecule electronic and thermoelectric device induced by light in a designed diarylethene molecule

Liang Ma,[1] Guangjun Tian,[1,*] and Jing-Tao Lü[2,†]

[1]*State Key Laboratory of Metastable Materials Science & Technology and Key Laboratory for Microstructural Material Physics of Hebei Province, School of Science, Yanshan University, Qinhuangdao 066004, People's Republic of China*

[2]*School of Physics and Wuhan National High Magnetic Field Center, Huazhong University of Science and Technology, 430074 Wuhan, People's Republic of China*

(Received 2 September 2022; accepted 10 October 2022; published 17 October 2022)

Tremendous efforts have been devoted to studying ordinary and novel properties in molecular-scale. Especially the reversible and controlled electrical and thermoelectric switches, which have been extensively studied experimentally and theoretically. They possess two distinct electronic and thermoelectric transport states actuated by external triggers, such as light, temperature, and electric field. Here, a photochromic diarylethene, linked to a nontriazatriangulene platform covalently, is studied by first-principles calculation. By means of density functional theory, we calculate the density of states and scanning tunneling microscope (STM) images of the designed diarylethene adsorbed on a Au(111) surface. Moreover, the thermoelectric transport properties of diarylethene-based molecular junction with a Au(111) electrode are studied systematically by using nonequilibrium Green's function transport formalism. We illustrate that due to the structure chang e of the designed diarylethene induced by light, the electronic and thermoelectric transport properties of the junction are completely different. Those differences can be visualized by the calculated electronic transmission eigenchannel and transport pathway. Furthermore, we demonstrate that the structure change of the designed diarylethene can be detected by STM experiments. The present study shows that the designed diarylethene could be a desirable candidate for electronic and thermoelectric molecular switch driven by light.

DOI: 10.1103/PhysRevB.106.165416

I. INTRODUCTION

Building electronic devices using individual molecules is one of the ultimate goals in molecular electronics [1–4]. The special functionalities of single molecular junctions could lead to new properties that are not possible to implement in conventional solid state devices. Therefore, molecular electronics provide a platform to investigate not only the basic questions in device miniaturization but also the interesting quantum phenomena, such as quantum interference [5–11], Coulomb blockade, Franck-Condon blockade, and Kondo effects [12–14]. More recently, an atomically precise gating strategy has been developed to manipulate the frontier orbitals of molecular components and switch the quantum interference between destructive and constructive states at the single molecular scale [15].

Single molecular devices can be well prepared by using scanning tunneling microscope break-junctions (STM-BJ), mechanically controllable break-junctions (MCBJ), electromigration break-junctions (EBJ), and so on. Moreover, one can characterize it's electrical conductance [16,17], thermal conductance [18], Seebeck coefficient [19–22], inelastic electron tunneling spectroscopy (IETS) [23], shot noise [24–27], delta-T noise [28], and so on. Very recently, a quantum form of electronic flicker noise in nanoscale conductors has been experimentally identified which revealed the relationship between quantum flicker noise and distribution of transmission channels [29].

The theoretical description of quantum transport in single molecular devices is an interesting and challenging problem. During the last two decades, the nonequilibrium Green's functions (NEGF) method combined with density functional theory (DFT), known as DFT-NEGF, has been recognized as one of the most powerful computational tools for simulating the transport properties of single molecular devices. It has been implemented in TRANSIESTA [30,31], Nanodcal [32], SMEAGOL [33], and many other packages [34–36]. Recently, hierarchical quantum master equation approach has been extended to evaluate the higher-order current cumulants in nanojunction [37]. Machine learning was also introduced to study the transport properties, achieving qualitative agreement with experiments [38]. Very recently, a semiclassical Langevin molecular dynamics method was employed to study the temperature-dependent thermal transport of single molecular junctions [39], in which both quantum statistics and anharmonic interaction are included within one theoretical framework.

In the field of molecular electronics, switchable electronic and thermoelectric devices have attracted extensive attention [40–45]. They are responsive to external stimuli, such as electric field, temperature, magnetic field, mechanical motion, and light. Among various stimuli, light possesses several

---

[*] tian@ysu.edu.cn

[†] jtlu@hust.edu.cn

advantages over others, namely its spatial and temporal control and low-cost. The smallest two-terminal molecular switches based on benzene-dithiolate molecules has already been proposed, in which lateral motion of the STM tip could cause benzene-dithiolate molecules to switch between a strongly conducting conformation and a weakly conducting conformation [40]. A fully reversible, two-mode, photo-switching that consists of a single diarylethene molecule has also been reported recently [45].

Some planar molecules, including porphyrins, diarylethene, and so on, tend to lie flat to maximize their interaction with the metal surface. To circumvent this shortcoming, here, a freestanding photo-switchable diarylethene (DAE) is placed vertically on a Au(111) surface using a triazatriangulene (TATA) platform as a anchoring group. Hereafter, we indicate this designed diarylethene molecule with DAE-TATA. The TATA platform could control the orientation of DAE to the surface and adjust the distance between neighboring molecules on the surface. It is proved by experiment that irradiated by UV and visible light alternatively, DAE-TATA can reversibly change between the ring-open and ring-closed configurations [46]. Meanwhile, the authors assembled the DAE-TATA into self-assembled monolayers on a Au surface. X-ray photoelectron spectroscopy was carried out and found the thickness of the monolayers will change after light irradiation, which suggested the structure isomerization process can still take place for the adsorbed system. One of the key reasons for the preserved activity of the molecule is the incorporation of the TATA base, which can be considered as a decoupling buffer that preserves the intrinsic properties of the DAE unit. DAE molecule has been proven to be a typical system for single molecular switch based on a light induced structural isomerization process [45,47] that also suggested the change of the molecule between the ring-closed and ring-open form could take place even when it was placed between electrodes. Here, the DAE molecule was covalently bonded to the TATA platform. The distance between the TATA platform and the two C atoms (∼8.3 Å), where ring-open and ring-closed happens, is much larger than CC bond length (∼1.4 Å). Thus, we think the structure of DAE-TATA could be changed by the application of light. Also, combining the calculated STM images, the structure change of DAE-TATA on a Au(111) surface can in principle be confirmed by future STM experiments.

In this work, transport calculations show that those two isomers have distinct electronic properties due to the change of the conjugated structure. Therefore, the freestanding DAE molecules supported by the TATA platform may be an ideal molecular system for high-performance molecular switch driven by light.

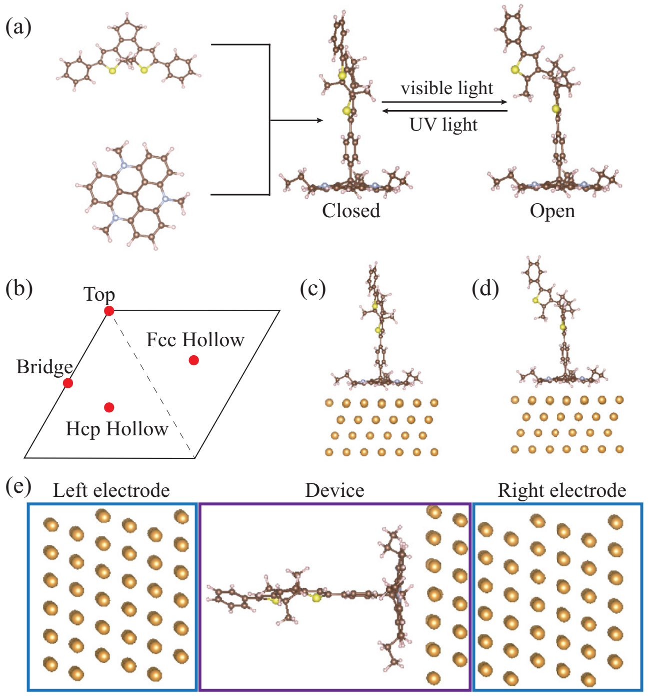

FIG. 1. Schematic representation of models considered in the present work. (a) Diarylethene (DAE), triazatriangulene (TATA), and designed diarylethene (DHA-TATA). Yellow balls are sulfur atoms. (b) Four adsorption sites on the Au(111) surface, named as Top, Bridge, Hcp Hollow, and Fcc Hollow, respectively. (c) and (d) indicate the adsorbed systems formed by DAE-TATA and Au(111). (e) Two-terminal DHA-TATA based molecular junction with a Au(111) electrode.

II. MODEL AND METHODS

The schematic representation of models considered in this work are shown in Fig. 1. As shown in Fig. 1(a), a freestanding photochromic DAE molecule, as a functional unit, is vertically linked to a TATA platform. In agreement with original DAE molecule, the conjugated structure of this designed molecule is still sensitive to light. Upon exposure to alternating visible and UV light, the structure of DAE-TATA can be reversibly converted between the ring-open and closed states.

The schematics of DAE-TATA adsorbed on a Au(111) surface are shown in Figs. 1(c) and 1(d). X-ray photoelectron spectroscopy and cyclic voltammetry were carried out confirming the formation of DAE-TATA monolayers on a Au substrate in Ref. [46]. The thickness of self-assembled monolayers, estimated from x-ray photoelectron spectroscopy measurements, is consistent with the theoretically calculated molecular length. It is indicated that the DAE-TATA is in favor of a vertical structure on the gold surface. Similarly, a “platform approach” has been proposed to mount porphyrins on a Au(111) surface [48] where the porphyrins stand upright in the middle of a TATA platform. Recently, a freestanding conjugated molecular wire has been placed vertically on a Au(111) surface using a platform molecule. Contacting by STM, the conductance of the freestanding molecule wire has been measured [49]. From the theoretical aspect, we show that the DAE molecule, supported by a TATA platform, can stand upright on a Au(111) surface. Here, based on the calculation results, we infer that it can also be detected by STM experiments.

According to the symmetry of a Au(111) surface, four adsorption sites should be take into account [see Fig. 1(b)]. Finally, we connect the DAE-TATA to a Au(111) electrode forming a two-terminal molecular junction, as can be seen in

Fig. 1(e). Its electronic and thermoelectric transport properties are fully studied in this work.

A. Electronic structure and STM image

The Vienna *ab initio* Simulation Package (VASP) is used to calculate the electronic structure and STM image of the adsorbed systems formed by DAE-TATA and Au(111) [50]. VASP is based on the projector-augmented wave method and a plane wave basis set. In our calculation, the Perdew-Burke-Ernzerhof (PBE) version of the generalized gradient approximation was chosen [51]. We adopt a four-layer slab of Au to model the Au(111) surface. Each atomic layer contains 36 (6×6) atoms. A vacuum space of 10 Å in the z direction was inserted to eliminate interactions between the nearest supercells. The van der Waals dispersive interaction was considered according to Grimme's DFT-D2 method [52]. The kinetic cut-off energy for the plane-waves basis was set to 400 eV. The convergence criterion of the self-consistent electronic loops was set to 10^{-6} eV. In order to get the optimized structure, the DAE-TATA and top two layers of Au(111) were relaxed, without any constraint, until the forces acting on each atom is lower than 0.01 eV/Å. The two bottom layers of the Au(111) slab were kept fixed. For sampling the three-dimensional Brillouin zone, the scheme proposed by Monkhorst and Pack was used [53]. Γ-point approximation was adopted to optimize the structure and calculate the STM image. For balance accuracy and efficiency, we use a $3 \times 3 \times 1$ $k$mesh to calculate the density of states (DOS) and projected density of states (PDOS).

The STM images were simulated by means of the Tersoff-Hamann scheme [54]. This scheme approximately links the STM tunneling current with the local density of states (LDOS). It can be written as follows:

$$I(V) \propto \int_{E_F}^{E_F+eV} \rho(\vec{r}, E)dE, \tag{1}$$

where $\rho(\vec{r}, E)$ is the LDOS. If those states are fully filled, the LDOS is equivalent to charge density of the states. Therefore, within the Tersoff-Hamann scheme, the STM image shows the partial charge density in the specified energy range.

B. Thermoelectric transport properties

The thermoelectric transport properties of the DAE-TATA-based molecular junction with a Au(111) electrode are calculated based on the nonequilibrium Green's function transport formalism (NEGF). Firstly, we relax the junction, as can be seen in Fig. 1(e), to get an optimized structure. For this purpose, VASP is used and the same parameters with previous electronic structure calculations are chosen. It is noteworthy that only the device region is relaxed and the left and right electrodes are fixed. Then, we calculate thermoelectric transport properties of the optimized junction. The transmission function was calculated by means of the TRANSIESTA and TBtrans DFT computer codes, in which DFT-NEGF scheme was implemented [30,31]. Throughout the TRANSIESTA calculation, we used a single-ζ plus polarization (SZP) basis set. To converge total energy, the cutoff energy was set to 200 Ry and the tolerance of density matrix was set to 10^{-5} eV.

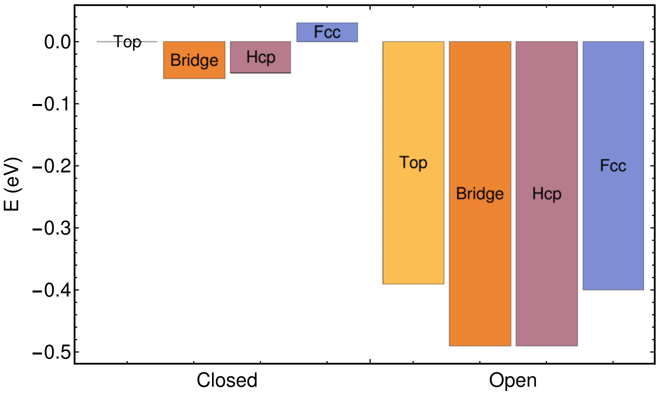

FIG. 2. Total energy of DAE-TATA adsorbed on a Au(111) surface with different adsorption sites.

Based on the zero-voltage transmission function, we calculate the thermoelectric transport coefficients in the framework

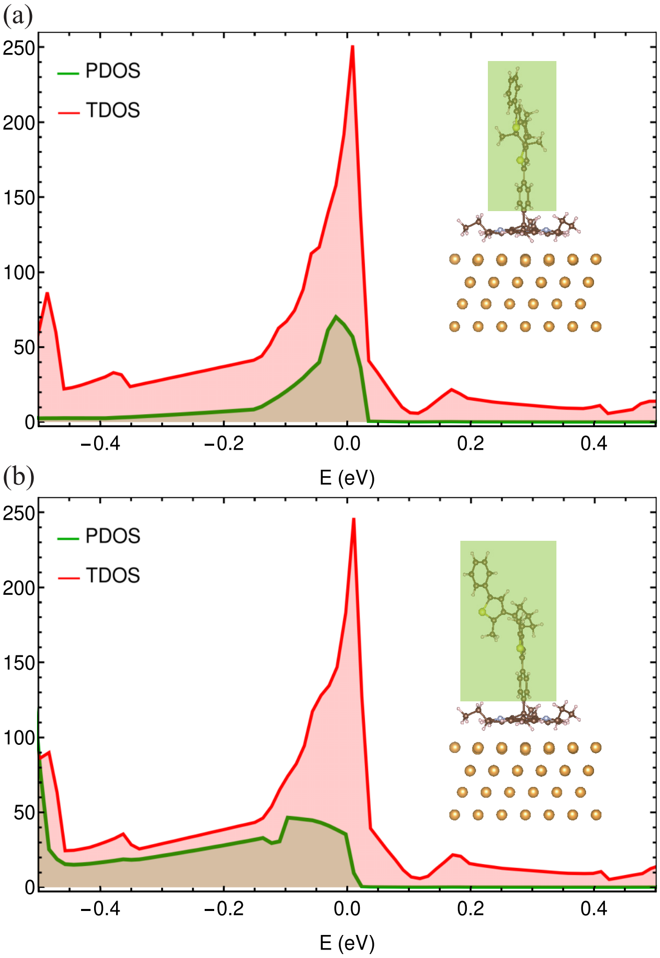

FIG. 3. Total density of states (TDOS) and projected density of states (PDOS) of DAE-TATA adsorbed on a Au(111) surface. (a) and (b) are corresponding to ring-closed and ring-open structure, respectively. Red line stands for TDOS and green line stands for PDOS. The insert shows the projected atoms.

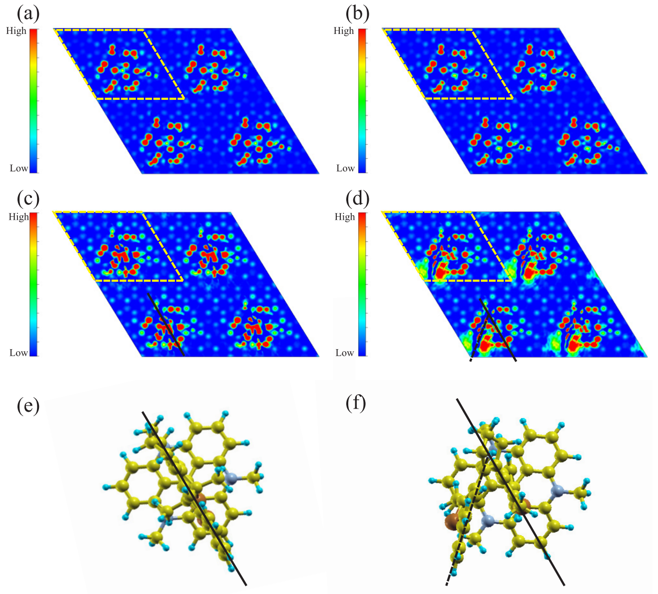

FIG. 4. STM images of the DAE-TATA molecule adsorbed on a Au(111) surface. (a), (b) ring-closed structure where the energy region, with respect to the Fermi level, is 0 ∼ 0.5 eV and −0.5 ∼ 0 eV, respectively. (c), (d) ring-open structure where the energy region, with respect to the Fermi level, is 0 ∼ 0.5 eV and −0.5 ∼ 0 eV, respectively. (e) and (f) show schematics of ring-closed and ring-open molecular structure for comparison.

of a linear response regime [55–60]. In this case, the electrical conductance G, electronic contribution to the thermal conductance κ_e, Seebeck coefficient S, and electronic contribution to the thermoelectric figure of merit ZT_{el} can be expressed as following:

$$G(\mu, T) \equiv \left.\frac{I}{\Delta V}\right|_{\Delta T=0} = e^2 L_0, \tag{2}$$

$$\kappa_e(\mu, T) \equiv \left.\frac{Q}{\Delta T}\right|_{I=0} = \frac{1}{T}\left(L_2 - \frac{{L_1}^2}{L_0}\right), \tag{3}$$

$$S(\mu, T) \equiv -\left.\frac{\Delta V}{\Delta T}\right|_{I=0} = -\frac{1}{eT}\frac{L_1}{L_0}, \tag{4}$$

$$ZT_{\mathrm{el}}(\mu, T) \equiv \frac{GS^2T}{\kappa} = \frac{L_1^2}{L_0L_2 - L_1^2}. \tag{5}$$

Here, the transport coefficients L_n can be defined as

$$L_n(\mu, T) = \frac{1}{h}\int_{-\infty}^{\infty}(E-\mu)^n \mathcal{T}(E)\left(-\frac{\partial f(E,\mu,T)}{\partial E}\right)dE. \tag{6}$$

C. Eigenchannels and Atomic Transmission

We also calculate the eigenchannels and atomic transmission to visualize the differences of thermoelectric transport coefficients between those two junctions. The eigenchannel can be obtained by diagonalizing the transmission matrix [61] and the atomic transmission can be calculated by sum of orbital transmissions of each atoms:

$$\mathcal{T}_{\alpha\beta} = \sum_{\nu\in\alpha}\sum_{\mu\in\beta}\mathcal{T}_{\nu\mu}. \tag{7}$$

Here, α and β stand for atoms. ν and μ stand for orbital of atoms. The eigenchannels and atomic transmission can be extracted by the "post-processing" code Inelastica [62] and SISL [63].

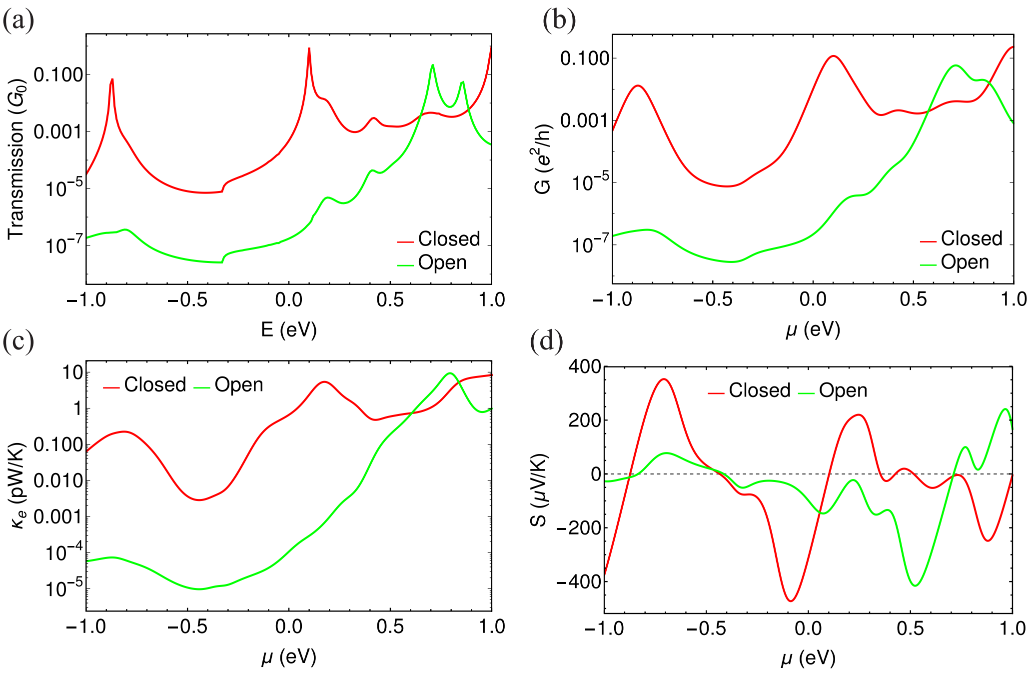

FIG. 5. Thermoelectric coefficients versus chemical potential of the single molecular junction. (a) Electronic transmission. (b) Electrical conductance (G). (c) Electronic thermal conductance (κ_e). (d) Seebeck coefficient (S).

Using the above methods, we calculated all the electronic structure of DAE-TATA on a Au(111) surface and the transport properties of the DAE-TATA-based junction in this present work.

III. RESULTS AND DISCUSSIONS

In this section the results of our calculations are presented. We start our discussion with the electronic structure of the adsorbed system formed by the DAE-TATA adsorbed on a Au(111) surface [see Figs. 1(c) and 1(d)], especially the total density of states (TDOS), projected density of states (PDOS), and STM image. Notably, there are four adsorption sites (marked by top, bridge, hcp hollow, and fcc hollow, respectively) should be taken into account due to the symmetry of a Au(111) surface, as can be seen in Fig. 1(b). We first check the stability of the four adsorption structures. As shown in Fig. 2, total energy (E) of the four adsorption structures were calculated. It's worth noting that we set the total energy of the ring-closed structure with top site to be zero for reference. As can be seen, for both ring-closed and ring-open structures, the structure within the bridge adsorption site has minimum total energy. Therefore, we mainly focus on this structure.

As is well known, the band structure of the supercell is complex due to the brillouin zone folding. However, we can still get some valuable information from the density of states (DOS). As shown in Fig. 3, the TDOS and PDOS of DAE-TATA, for both ring-closed and ring-open structures, adsorbed on a Au(111) surface, are calculated. Here, the PDOS indicates that the density of states are projected to the DAE molecule [marked by the green area in the insert figure of Fig. 3]. We can see that, the TODS of these two structures are nearly the same in our calculations. Therefore, the structure changing from ring-closed to ring-open has little effect on the TODS. However, the PDOS of these two structures are different. This is reasonable for the structure changes taking place in DAE molecules. Notably, the PDOS are primarily localized below the Fermi level for both structures. In contrast, the PDOS is approaching zero above the Fermi level. These results can be evidenced by the STM experiment.

The calculation results of the STM image based on the Tersoff-Hamann scheme [54] are presented in Fig. 4. We enlarged the STM image by two times along the *xy* direction to demonstrate clearly. The supercell used in our calculations is marked by the yellow dashed diamond box in the illustration. The STM images of the ring-closed structure are given in Figs. 4(a) and 4(c), in which, the energy region relative to the Fermi level are $0 \sim 0.5\,\mathrm{eV}$ and $-0.5 \sim 0\,\mathrm{eV}$, respectively. Similarly, Figs. 4(b) and 4(d) are corresponding to ring-open structure whose energy region relative to the Fermi level are $0 \sim 0.5\,\mathrm{eV}$ and $-0.5 \sim 0\,\mathrm{eV}$. From Figs. 4(a) and 4(b) we could see that the STM patterns are mainly coming to the TATA molecule. Namely, for both ring-closed and ring-open structures, the TATA molecule made a significant contribution to the STM image in energy region $0 \sim 0.5\,\mathrm{eV}$. The STM images given in Figs. 4(c) and 4(d) consistently show that additional patterns appear in energy region $0.5 \sim 0\,\mathrm{eV}$. In fact, those patterns are triggered by DAE molecules. Making a close comparison between Figs. 4(c) and 4(d), we will see that the six-membered ring of the DAE molecule changes from closed to open. This is indicated by the black solid and dashed line in Figs. 4(c) and 4(d). Corresponding to the changing of STM patterns, the structure changing of DAE molecules was shown in Figs. 4(e) and 4(f). Together with the calculated TDOS and PDOS, the STM images show that the structure change of the DAE molecule can be detected by STM experiment. However, it is biasdependent. According to our estimates, the bias used in the STM experiment has to ensure that an energy area below the Fermi energy level, such as -0.5 ∼ 0 eV in our calculation, should be included.

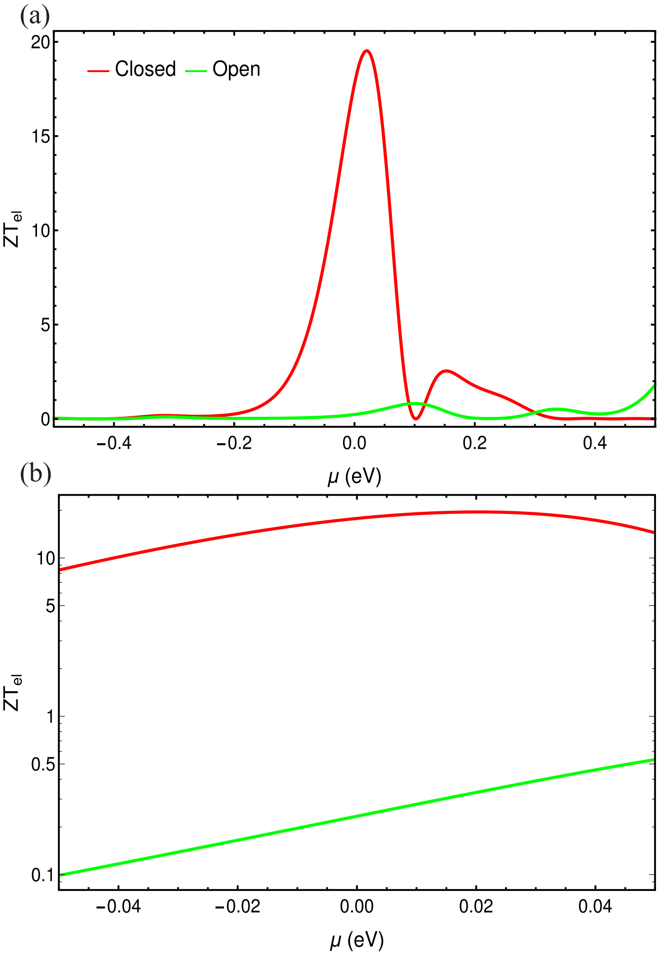

FIG. 6. (a) Electronic contribution to the thermoelectric figure of merit(ZT_{el}) versus chemical potential. (b) is the same as (a) but with logarithmic scale and mainly focuses on the vicinity of the Fermi level.

We are now in the position to discuss the thermoelectric transport properties of the DAE-TATA-based molecular junction with a Au(111) electrode [see Fig. 1(e)]. By means of the method described in Sec. II B, the thermoelectric coefficients are calculated [see Fig. 5]. As illustrated in Fig. 5(a), the transmission function of the ring-closed based junction is noticeably bigger than that of the ring-open based junction in a wide range of energies. Electrical conductance and electronic thermal conductance for the two junctions behave in the same way [see Figs. 5(b) and 5(c)]. At the Fermi level, the electrical conductance of ring-closed based junction is nearly two orders of magnitude greater than that of ring-open based junction.

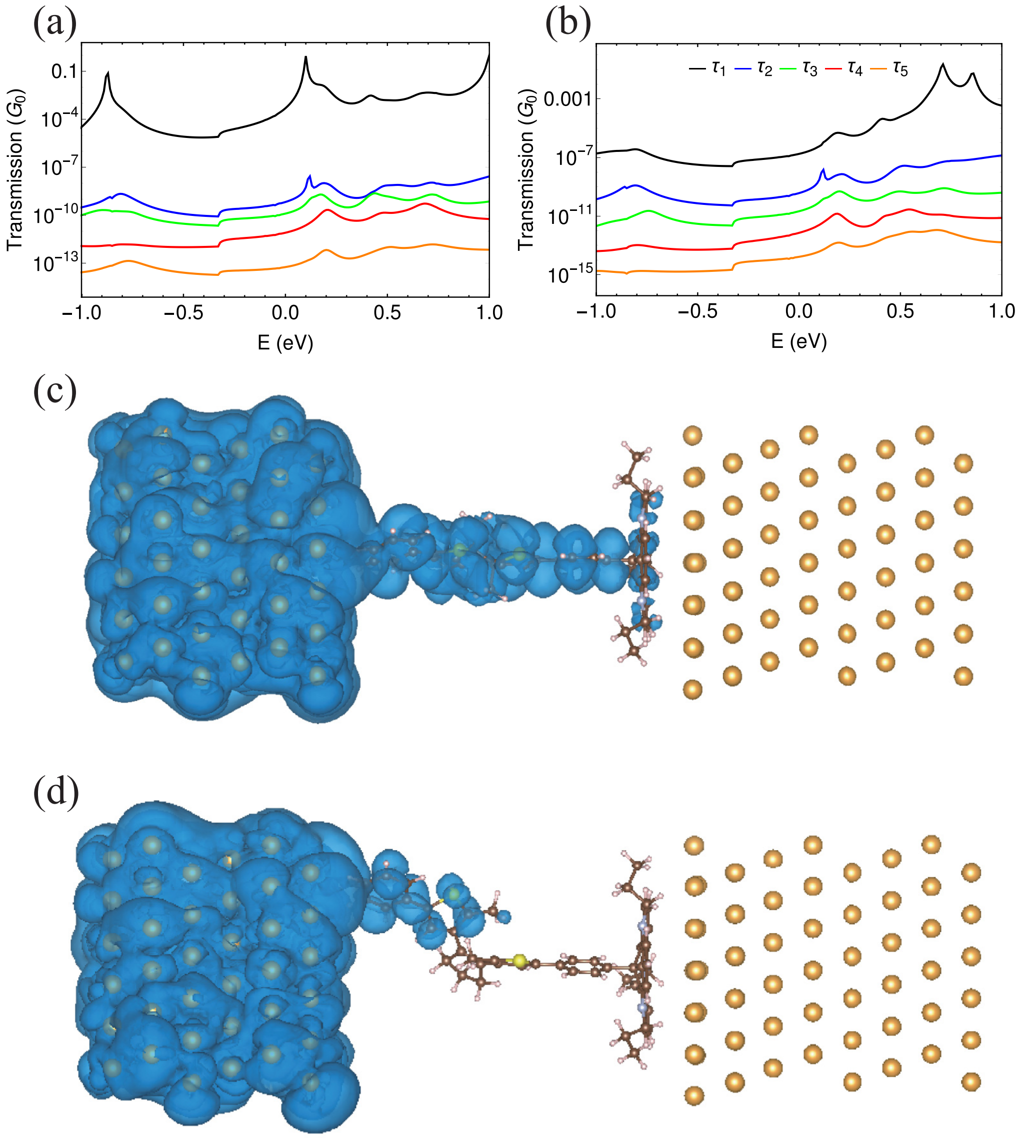

FIG. 7. (a) and (b) are the transmission decomposed in eigenchannels for ring-closed and ring-open junctions, respectively. (c) and (d) are the real-space distribution of eigenchannels for ring-closed and ring-open junctions, respectively. The isosurface was set to 10^{-5}.

As a result, adjusting the electrical conductance of this DAE-TATA-based junction by light looks promising. Significantly, the Seebeck coefficient of a ring-closed based junction is larger than that of a ring-open based junction near the Fermi level. The larger power factor of ring-closed based junction will lead to larger thermoelectric figure of merit. This can be evidenced by Fig. 6.

In Fig. 6(a), we plot the electronic contribution to the thermoelectric figure of merit of the two junctions. We could see that the thermoelectric figure of merit of the ring-closed junction is dramatically greater than that of the ring-open junction near the Fermi level. This can also be seen clearly in Fig. 6(b). Where we show the thermoelectric figure of merit of the two junctions in logarithmic scale within energy region $[-0.05 \sim 0.05]$ eV. In this region, the thermoelectric figure of merit of the ring-closed based junction is roughly two orders of magnitude greater than that of the ring-open based junction. DFT is known to overestimate the conductance due to the underestimation of the HOMO-LUMO gap. Advanced methods, for example self-consistent GW approximation, have been proposed to correct the transport properties of nanoscale systems [64,65]. Good agreement between experiments and calculations have been reached by means of those methods. However, we mainly focused on the distinction of the thermoelectric transport properties for those two isomers. The absolute value of the thermoelectric coefficients played a relatively minor role in this work. We expect that our main results are intact by ignoring the conductance overestimation by DFT. Therefore, from a theoretical perspective, we confirmed that the DAE-TATA-based molecular junction could be a potential candidate for light-driven switchable electronic and thermoelectric molecular devices.

Finally, we try to confirm the differences of electronic transport between the ring-closed and the ring-open based molecular junction by the calculated eigenchannels and atomic transmission. The eigenchannels of those two junctions are shown in Fig. 7. When comparing the calculated findings in Figs. 7(a) and 7(b) and Fig. 5(a), we clearly ob-

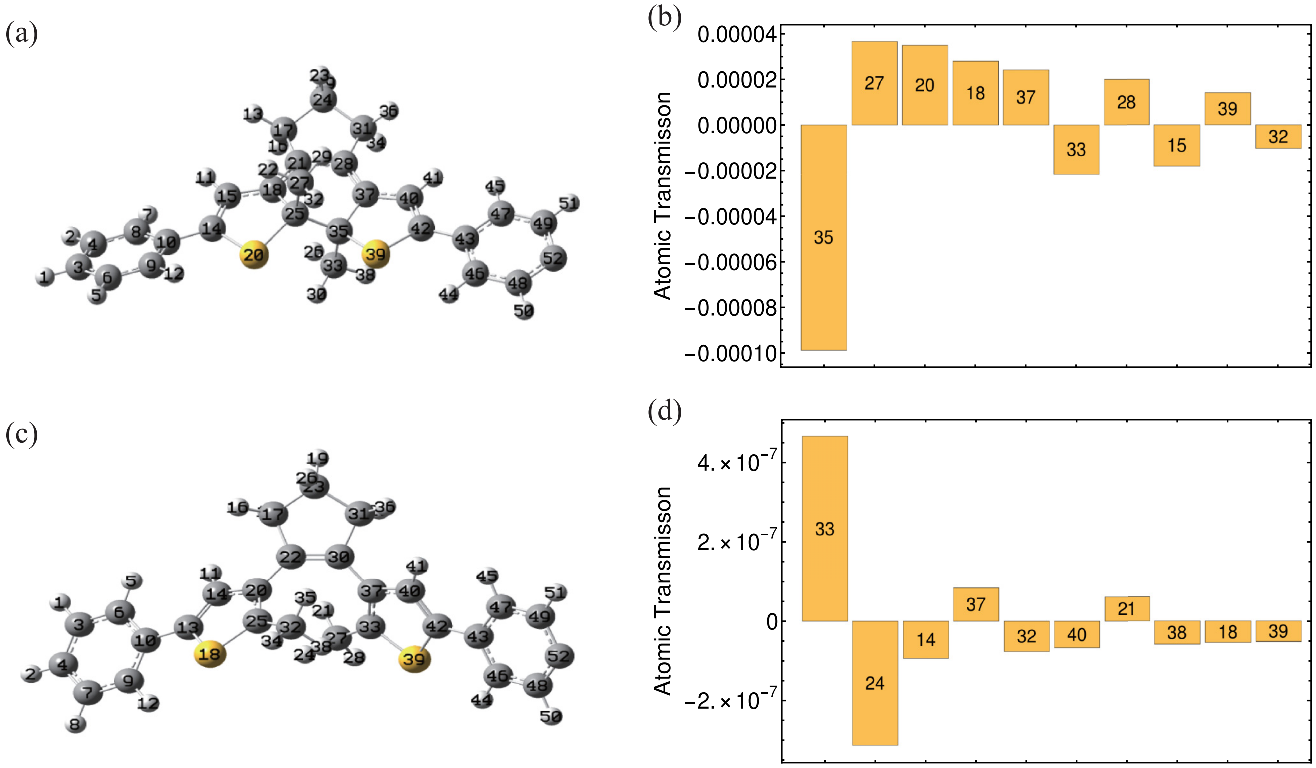

FIG. 8. Atomic transmission of the junction. (a) Schematic representation of the ring-closed DAE molecule involved in the junction. where each atom was assigned a number for classification. (b) Atomic transmission from atom 25 to others for ring-closed structure. (c) is the same as (a) but for ring-open structure. (d) Atomic transmission from atom 25 to others for ring-open structure. The positive stands for outflow and negative stands for inflow. Yellow balls are sulfur atoms.

serve that the electronic transmission of the two junctions is indeed governed by the first eigenchannel(τ_1). It can be probed by the shot noise experiment. Therefore, we show the real-space distribution of τ_1 for the ring-open based junction and the ring-closed based junction in Figs. 7(c) and 7(d). Due to breaking of the CC bond and the deformation of the DAE molecule, the real-space distribution of τ_1 for the ring-open based junction is more localized than that of the ring-closed based junction. As a result, the ring-closed based junction is more efficient than the ring-open based junction in terms of electron transport.

The atomic transmission under zero bias was also calculated to inspect the effects of DAE molecule deformation on its electron transport. By projecting the total transmission onto each atom, the atomic transmission was obtained. The results are shown in Fig. 8. The structure of the open and the closed DAE molecule contained in the molecular junctions is depicted in Figs. 8(a) and 8(c). Here the atoms are sorted by their position, and each atom was assigned a number. We mainly focus on the C atoms where the CC bond was breaking. For the closed structure, those two C atoms are indicated by 25 and 35, respectively. Among all of the atomic transmission from atom 25 to other atoms, we pick up some main contributions to display in Fig. 8(b). The positive stands for outflow from atom 25 to others, and negative stands for inflow. It is noteworthy that, for each atom, the sum of inflow and outflow should be zero. From Fig. 8(b), we find that among all of the electron transmission pathways through atom 25, the one between atom 25 and 35 is the most important. This means that, electrons mainly transport through the CC bond formed by the atoms 25 and 35. For the open structure, the CC bond is breaking. Notably, those two C atoms are indicate by 25 and 33, as shown in Fig. 8(c). The electrons still transport through the same pathway with the closed structure, as is shown in Fig. 8(d). However, comparing Figs. 8(b) and 8(d), it is obvious that the quantity of it's transmission is nearly two orders of magnitude smaller than that of the closed structure. Therefore, by analyzing transmission, eigenchannels, and the atomic transmission, we demonstrate that DAE molecule structure changing induced by light leads to a significant difference in molecular conductance.

IV. CONCLUSIONS

The present work was designed to investigate the electronic structure of an adsorption system made up of DAE-TATA molecule and a Au(111) surface. More importantly, the thermoelectric transport properties of the DAE-TATA-based single molecular junction were systematically inspected by using first-principles calculations based on the DFT-NEGF methodologies. We find that the structure change of the DAE molecule induced by light can be detected by the STM experiment in single molecule levels. Moreover, combining the calculated thermoelectric transport coefficients, electronic transport eigenchannel, and atomic transmission, we demonstrate that the electrical conductance, the Seebeck coefficient, and the electronic contribution to thermoelectric figure of merit of the molecular junction in the ring-closed form is nearly two orders of magnitude greater than that of ring-open form near the Fermi level. These results suggest that DAE-TATA molecule could be a desirable candidate for single molecular switch and single molecular thermoelectric devices controlled by light.

ACKNOWLEDGMENTS

This work was supported by the National Natural Science Foundation of China (Grants No. 62201494, No. 21873033, No. 21973081, and No. 22273029). We thank the National Supercomputing Center in Shanghai for providing computational resources.

[1] A. Aviram and M. A. Ratner, Molecular rectifiers, Chem. Phys. Lett. **29**, 277 (1974).

[2] D. Xiang, X. Wang, C. Jia, T. Lee, and X. Guo, Molecular-scale electronics: From concept to function, Chem. Rev. **116**, 4318 (2016).

[3] N. Xin, J. Guan, C. Zhou, X. Chen, C. Gu, Y. Li, M. A. Ratner, A. Nitzan, J. F. Stoddart, and X. Guo, Concepts in the design and engineering of single-molecule electronic devices, Nat. Rev. Phys. **1**, 211 (2019).

[4] F. Evers, R. Korytár, S. Tewari, and J. M. van Ruitenbeek, Advances and challenges in single-molecule electron transport, Rev. Mod. Phys. **92**, 035001 (2020).

[5] K. K. Saha, B. K. Nikolić, V. Meunier, W. Lu, and J. Bernholc, Quantum-Interference-Controlled Three-Terminal Molecular Transistors Based on a Single Ring-Shaped Molecule Connected to Graphene Nanoribbon Electrodes, Phys. Rev. Lett. **105**, 236803 (2010).

[6] T. Markussen, R. Stadler, and K. S. Thygesen, The relation between structure and quantum interference in single molecule junctions, Nano Lett. **10**, 4260 (2010).

[7] S. Ballmann, R. Härtle, P. B. Coto, M. Elbing, M. Mayor, M. R. Bryce, M. Thoss, and H. B. Weber, Experimental Evidence for Quantum Interference and Vibrationally Induced Decoherence in Single-Molecule Junctions, Phys. Rev. Lett. **109**, 056801 (2012).

[8] H. Vazquez, R. Skouta, S. Schneebeli, M. Kamenetska, R. Breslow, L. Venkataraman, and M. S. Hybertsen, Probing the conductance superposition law in single-molecule circuits with parallel paths, Nat. Nanotechnol. **7**, 663 (2012).

[9] C. M. Guédon, H. Valkenier, T. Markussen, K. S. Thygesen, J. C. Hummelen, and S. J. v. d. Molen, Observation of quantum interference in molecular charge transport, Nat. Nanotechnol. **7**, 305 (2012).

[10] C. J. Lambert, Basic concepts of quantum interference and electron transport in single-molecule electronics, Chem. Soc. Rev. **44**, 875 (2015).

[11] S. Gunasekaran, J. E. Greenwald, and L. Venkataraman, Visualizing quantum interference in molecular junctions, Nano Lett. **20**, 2843 (2020).

[12] H. Park, J. Park, A. K. L. Lim, E. H. Anderson, A. P. Alivisatos, and P. L. McEuen, Nanomechanical oscillations in a single-C_{60} transistor, Nature **407**, 57 (2000).

[13] J. Koch and F. von Oppen, Franck-Condon Blockade and Giant Fano Factors in Transport through Single Molecules, Phys. Rev. Lett. **94**, 206804 (2005).

[14] W. Liang, M. P. Shores, M. Bockrath, J. R. Long, and H. Park, Kondo resonance in a single-molecule transistor, Nature **417**, 725 (2002).

[15] C. Tang, L. Huang, S. Sangtarash, M. Noori, H. Sadeghi, H. Xia, and W. Hong, Reversible switching between destructive and constructive quantum interference using atomically precise chemical gating of single-molecule junctions, J. Am. Chem. Soc. **143**, 9385 (2021).

[16] M. A. Reed, C. Zhou, C. J. Muller, T. P. Burgin, and J. M. Tour, Conductance of a molecular junction, Science **278**, 252 (1997).

[17] B. Xu and N. J. Tao, Measurement of single-molecule resistance by repeated formation of molecular junctions, Science **301**, 1221 (2003).

[18] L. Cui, S. Hur, Z. A. Akbar, J. C. Klöckner, W. Jeong, F. Pauly, S.-Y. Jang, P. Reddy, and E. Meyhofer, Thermal conductance of single-molecule junctions, Nature **572**, 628 (2019).

[19] P. Reddy, S.-Y. Jang, R. A. Segalman, and A. Majumdar, Thermoelectricity in molecular junctions, Science **315**, 1568 (2007).

[20] J. R. Widawsky, P. Darancet, J. B. Neaton, and L. Venkataraman, Simultaneous determination of conductance and thermopower of single molecule junctions, Nano Lett. **12**, 354 (2012).

[21] C. Evangeli, K. Gillemot, E. Leary, M. T. González, G. Rubio-Bollinger, C. J. Lambert, and N. Agraït, Engineering the thermopower of C_{60} molecular junctions, Nano Lett. **13**, 2141 (2013).

[22] P. Gehring, J. K. Sowa, C. Hsu, J. de Bruijckere, M. van der Star, J. J. Le Roy, L. Bogani, E. M. Gauger, and H. S. J. van der Zant, Complete mapping of the thermoelectric properties of a single molecule, Nat. Nanotechnol. **16**, 426 (2021).

[23] J. G. Kushmerick, J. Lazorcik, C. H. Patterson, R. Shashidhar, D. S. Seferos, and G. C. Bazan, Vibronic contributions to charge transport across molecular junctions, Nano Lett. **4**, 639 (2004).

[24] O. Tal, M. Krieger, B. Leerink, and J. M. van Ruitenbeek, Electron-vibration interaction in single-molecule junctions: From contact to tunneling regimes, Phys. Rev. Lett. **100**, 196804 (2008).

[25] M. Kiguchi, O. Tal, S. Wohlthat, F. Pauly, M. Krieger, D. Djukic, J. C. Cuevas, and J. M. van Ruitenbeek, Highly Conductive Molecular Junctions Based on Direct Binding of Benzene to Platinum Electrodes, Phys. Rev. Lett. **101**, 046801 (2008).

[26] M. A. Karimi, S. G. Bahoosh, M. Herz, R. Hayakawa, F. Pauly, and E. Scheer, Shot noise of 1,4-benzenedithiol single-molecule junctions, Nano Lett. **16**, 1803 (2016).

[27] S. Larocque, E. Pinsolle, C. Lupien, and B. Reulet, Shot Noise of a Temperature-Biased Tunnel Junction, Phys. Rev. Lett. **125**, 106801 (2020).

[28] O. S. Lumbroso, L. Simine, A. Nitzan, D. Segal, and O. Tal, Electronic noise due to temperature differences in atomic-scale junctions, Nature **562**, 240 (2018).

[29] O. Shein-Lumbroso, J. Liu, A. Shastry, D. Segal, and O. Tal, Quantum Flicker Noise in Atomic and Molecular Junctions, Phys. Rev. Lett. **128**, 237701 (2022).

[30] M. Brandbyge, J.-L. Mozos, P. Ordejón, J. Taylor, and K. Stokbro, Density-functional method for nonequilibrium electron transport, Phys. Rev. B **65**, 165401 (2002).

[31] N. Papior, N. Lorente, T. Frederiksen, A. García, and M. Brandbyge, Improvements on non-equilibrium and transport Green function techniques: The next-generation transiesta, Comput. Phys. Commun. **212**, 8 (2017).

[32] J. Taylor, H. Guo, and J. Wang, *Ab initio* modeling of quantum transport properties of molecular electronic devices, Phys. Rev. B **63**, 245407 (2001).

[33] A. R. Rocha, V. M. García-Suárez, S. Bailey, C. Lambert, J. Ferrer, and S. Sanvito, Spin and molecular electronics in atomically generated orbital landscapes, Phys. Rev. B **73**, 085414 (2006).

[34] T. Ozaki, K. Nishio, and H. Kino, Efficient implementation of the nonequilibrium Green function method for electronic transport calculations, Phys. Rev. B **81**, 035116 (2010).

[35] J. Chen, K. S. Thygesen, and K. W. Jacobsen, *Ab initio* nonequilibrium quantum transport and forces with the real-space projector augmented wave method, Phys. Rev. B **85**, 155140 (2012).

[36] J. Ferrer, C. J. Lambert, V. M. García-Suárez, D. Z. Manrique, D. Visontai, L. Oroszlany, R. Rodríguez-Ferradás, I. Grace, S. W. D. Bailey, K. Gillemot, H. Sadeghi, and L. A. Algharagholy, GOLLUM: A next-generation simulation tool for electron, thermal and spin transport, New J. Phys. **16**, 093029 (2014).

[37] C. Schinabeck and M. Thoss, Hierarchical quantum master equation approach to current fluctuations in nonequilibrium charge transport through nanosystems, Phys. Rev. B **101**, 075422 (2020).

[38] M. Bürkle, U. Perera, F. Gimbert, H. Nakamura, M. Kawata, and Y. Asai, Deep-Learning Approach to First-Principles Transport Simulations, Phys. Rev. Lett. **126**, 177701 (2021).

[39] G. Li, B.-Z. Hu, N. Yang, and J.-T. Lü, Temperature-dependent thermal transport of single molecular junctions from semiclassical langevin molecular dynamics, Phys. Rev. B **104**, 245413 (2021).

[40] E. G. Emberly and G. Kirczenow, The Smallest Molecular Switch, Phys. Rev. Lett. **91**, 188301 (2003).

[41] B.-Y. Choi, S.-J. Kahng, S. Kim, H. Kim, H. W. Kim, Y. J. Song, J. Ihm, and Y. Kuk, Conformational Molecular Switch of the Azobenzene Molecule: A Scanning Tunneling Microscopy Study, Phys. Rev. Lett. **96**, 156106 (2006).

[42] M. J. Comstock, N. Levy, A. Kirakosian, J. Cho, F. Lauterwasser, J. H. Harvey, D. A. Strubbe, J. M. J. Fréchet, D. Trauner, S. G. Louie, and M. F. Crommie, Reversible Photomechanical Switching of Individual Engineered Molecules at a Metallic Surface, Phys. Rev. Lett. **99**, 038301 (2007).

[43] S. Y. Quek, M. Kamenetska, M. L. Steigerwald, H. J. Choi, S. G. Louie, M. S. Hybertsen, J. B. Neaton, and L. Venkataraman, Mechanically controlled binary conductance switching of a single-molecule junction, Nat. Nanotechnol. **4**, 230 (2009).

[44] F. Mohn, J. Repp, L. Gross, G. Meyer, M. S. Dyer, and M. Persson, Reversible Bond Formation in a Gold-Atom–Organic-Molecule Complex as a Molecular Switch, Phys. Rev. Lett. **105**, 266102 (2010).

[45] C. Jia, A. Migliore, N. Xin, S. Huang, J. Wang, Q. Yang, S. Wang, H. Chen, D. Wang, B. Feng, Z. Liu, G. Zhang, D.-H. Qu, H. Tian, M. A. Ratner, H. Q. Xu, A. Nitzan, and X. Guo, Covalently bonded single-molecule junctions with stable and reversible photoswitched conductivity, Science **352**, 1443 (2016).

[46] Q. Wang, L. Ma, Z. Liu, X. Zhang, Z. Zhang, Z. Shangguan, X. Huang, Y. Liu, J. Lv, H. Zhang, L. Chi, and T. Li, Triazatriangulene platform for self-assembled monolayers of free-standing diarylethene, Sci. China Mater. **61**, 1345 (2018).

[47] A. C. Whalley, M. L. Steigerwald, X. Guo, and C. Nuckolls, Reversible switching in molecular electronic devices, J. Am. Chem. Soc. **129**, 12590 (2007).

[48] F. L. Otte, S. Lemke, C. Schütt, N. R. Krekiehn, U. Jung, O. M. Magnussen, and R. Herges, Ordered monolayers of free-standing porphyrins on gold, J. Am. Chem. Soc. **136**, 11248 (2014).

[49] T. Jasper-Tönnies, A. Garcia-Lekue, T. Frederiksen, S. Ulrich, R. Herges, and R. Berndt, Conductance of a Freestanding Conjugated Molecular Wire, Phys. Rev. Lett. **119**, 066801 (2017).

[50] G. Kresse and J. Furthmüller, Efficient iterative schemes for ab initio total-energy calculations using a plane-wave basis set, Phys. Rev. B **54**, 11169 (1996).

[51] J. P. Perdew, K. Burke, and M. Ernzerhof, Generalized Gradient Approximation Made Simple, Phys. Rev. Lett. **77**, 3865 (1996).

[52] S. Grimme, Semiempirical GGA-type density functional constructed with a long-range dispersion correction, J. Comput. Chem. **27**, 1787 (2006).

[53] H. J. Monkhorst and J. D. Pack, Special points for brillouin-zone integrations, Phys. Rev. B **13**, 5188 (1976).

[54] J. Tersoff and D. R. Hamann, Theory and Application for the Scanning Tunneling Microscope, Phys. Rev. Lett. **50**, 1998 (1983).

[55] K. Esfarjani, M. Zebarjadi, and Y. Kawazoe, Thermoelectric properties of a nanocontact made of two-capped single-wall carbon nanotubes calculated within the tight-binding approximation, Phys. Rev. B **73**, 085406 (2006).

[56] L. Ma, L.-L. Nian, and J.-T. Lü, Design and optimization of a heat engine based on a porphyrin single-molecule junction with graphene electrodes, Phys. Rev. B **101**, 045410 (2020).

[57] J. Ren, J.-X. Zhu, J. E. Gubernatis, C. Wang, and B. Li, Thermoelectric transport with electron-phonon coupling and electron-electron interaction in molecular junctions, Phys. Rev. B **85**, 155443 (2012).

[58] G. Bevilacqua, G. Grosso, G. Menichetti, and G. Pastori Parravicini, Thermoelectric efficiency of nanoscale devices in the linear regime, Phys. Rev. B **94**, 245419 (2016).

[59] C. M. Finch, V. M. García-Suárez, and C. J. Lambert, Giant thermopower and figure of merit in single-molecule devices, Phys. Rev. B **79**, 033405 (2009).

[60] J. P. Bergfield and C. A. Stafford, Thermoelectric signatures of coherent transport in single-molecule heterojunctions, Nano Lett. **9**, 3072 (2009).

[61] M. Paulsson and M. Brandbyge, Transmission eigenchannels from nonequilibrium Green's functions, Phys. Rev. B **76**, 115117 (2007).

[62] T. Frederiksen, M. Paulsson, M. Brandbyge, and A.-P. Jauho, Inelastic transport theory from first principles: Methodology

and application to nanoscale devices, Phys. Rev. B **75**, 205413 (2007).

[63] N. Papior *et al.*, zerothi/sisl: v0.11.0 (2021), https://zenodo.org/record/4544334.

[64] M. Strange, C. Rostgaard, H. Häkkinen, and K. S. Thygesen, Self-consistent GW calculations of electronic transport in thiol- and amine-linked molecular junctions, Phys. Rev. B **83**, 115108 (2011).

[65] V. M. García-Suárez and C. J. Lambert, First-principles scheme for spectral adjustment in nanoscale transport, New J. Phys. **13**, 053026 (2011).